Electrocardiographic imaging including intracardiac information to achieve accurate global mapping during atrial fibrillation

Miguel Ángel Cámara-Vázquez[a,*],   Ismael Hernández-Romero[a],   Miguel Rodrigo[c],
Felipe Alonso-Atienza[a],   Carlos Figuera[a],   Eduardo Morgado-Reyes[a],   Felipe Atienza[b],
María S. Guillem[c],   Andreu M. Climent[c,*] and   Óscar Barquero-Pérez[a,**]

[a]Signal Theory and Communications and Telematic Systems and Computation Department, Rey Juan Carlos University, Camino del Molino 5, 28942 Fuenlabrada, Madrid, Spain
[b]Gregorio Marañón Health Research Institute, CIBERCV, Gregorio Marañón General University Hospital, Medicine Faculty, Complutense University of Madrid, C/Dr Esquerdo 46, 28007 Madrid, Spain
[c]ITACA Institute, Universitat Politècnica de València, Camí de Vera s/n, 46022 València, Spain

ARTICLE INFO

Keywords:
Atrial fibrillation
ECG imaging
Inverse problem
Epicardial potentials
Dominant frequency
Rotor location

ABSTRACT

Atrial fibrillation (AF) is characterized by complex and irregular propagation patterns. Noninvasive electrocardiographic imaging (ECGI) has been tested during AF conditions with promising results. However, current regularization methods face important challenges in this type of unstable electrical activity scenarios. Combination of intracardiac and non-invasive simultaneous recordings could improve ECGI performance and allow real-time global mapping of complex AF patterns. In this work, we propose an ECGI method that incorporates intracardiac measurements as a constraint in a reformulation of the classical Tikhonov method. We used realistic mathematical models of atria and torso that simulates a wide number of epicardial electrical activity patterns. Body surface potentials were obtained from simulated electrograms (EGMs) by using Boundary Element Method and corrupted with Gaussian noise. Epicardial potentials were estimated using inverse problem with Tikhonov regularization, including intracavitary information as a second constraint. Results showed that first-order Constrained Tikhonov formulation provided more reliable reconstructions than the classical Tikhonov approach in AF conditions using at least 32 uniformly distributed endocardial EGMs (CC between 0.87 and 0.28, depending on the AF complexity). Constrained Tikhonov provided more accurate spatial mass functions (SMF) of PS locations (CCSMF between 0.24 and 0.86). This methodology was tested on real patient data, obtaining a mean DF RMSE of 0.85 Hz, outperforming the classical Tikhonov approach. Limitations of this study include the fact that the model considered endocardium and epicardium as a single layer. Further research will include endocardium-epicardium bilayer model approximations and validation using more real patient data.

1. Introduction

Atrial fibrillation (AF) is the most common type of arrhythmia in clinical practice. AF affects more than 33 million patients in the world [9]. Patients with this condition have an increased risk of suffering embolism, cardiac failure, stroke and, in the worst of cases, death [19].

One of the clinical goals in AF patients is to restore sinus rhythm, usually by ablation. Main targets of ablation are AF onset locations and drivers responsible for AF perpetuation [22]. Although novel signal processing methods has been proposed to identify rotor pivot points using optical mapping [1], most studies suggested that stable sites of phase singularities (PS) are responsible for maintaining AF. In previous human in vivo research, several clinical studies have proposed different strategies to locate AF drivers and guide pulmonary veins isolation (PVI). On the one hand, by performing an invasive mapping procedure [33, 27, 34], and, on the other hand, by performing a noninvasive mapping using ECG Imaging (ECGI) [26, 25, 16]. However, PS-guided ablation is suggested as a reliable alternative in persistent AF cases, where PVI has a low success rate [14, 47].

ECGI has been previously proposed to effectively reconstruct the electrophysiological activity on the heart surface, solving the spatio-temporal limitations of classical ECG, by using a non-invasive recording of body surface potentials (BSP) [7, 24]. ECGI combines both numerical modeling of the bioelectric properties of the thorax and signal processing. However, the inverse problem of ECGI is ill-posed because the propagation between the epicardium and the torso implies information loss [46], mainly due to signal attenuation. Moreover, BSP are also blurred compared to the signals on the heart due to the laws of electromagnetic field theory. Regularization methods are needed to obtain reliable and stable epicardial potential reconstructions [38, 53, 39, 29, 31], which, in turn allow us to identify dominant high-frequency regions [40], activation sequences [13, 42] or arrhythmogenic substrates [48].

The inverse problem of ECGI has been recently used to estimate and analyze irregular propagation patterns. For example, phase mapping approaches have been proposed to analyze spatio-temporal characteristics of AF-related signals [46]. However, ECGI has not been validated during these irregular propagation patterns, and AF reconstructed patterns are

*Corresponding author
**Principal corresponding author
✉ miguelangel.camara@urjc.es (Miguel Ángel Cámara-Vázquez);
andreu.climent@gmail.com (Andreu M. Climent); oscar.barquero@urjc.es (
Óscar Barquero-Pérez)
ORCID(s): 0000-0002-1861-1585 (Miguel Ángel Cámara-Vázquez)

usually simpler than complex patterns recorded directly in the epicardium [12]. These results are partially related to the smoothness imposed by regularization. Despite these limitations, ECGI has been demonstrated as a promising tool to identify AF drivers and guide ablation procedures [25].

During AF ablation procedures, several catheters are introduced in the atrial chambers. Depending on the ablation strategy, the number of recorded EGMs may vary from 8 to 128 simultaneous signals [33]. Despite the number of intracardiac signals, the complex atrial anatomy and the large distance between catheter sensors (up to 1-2 cm) limits the ability of intracardiac mapping systems to characterize the global activity of AF [36].

Including any available *a priori* information during the electrophysiological study (EPS) may improve the estimation of electrical activity on the heart [38, 6, 50]. Furthermore, combining non-invasive and invasive recordings during the ablation procedures may overcome some of the limitations of each individual technique and lead to more accurate identification of AF drivers. One of the main challenges is to propose a method that is able to take into account intracavitary measurements. In this work, we are proposing a new Tikhonov-based formulation for inverse problem that includes EGM-based intracavitary measurements obtained from the endocardium, simultaneously to BSP.

The remaining of the paper is organized as follows. In Section 2 we introduce the computational models and patient data used for this study, the Tikhonov-based regularization algorithms, and the performance metrics. Final results are explained and discussed in Section 3 and, finally, in Section 4 main conclusions are presented.

2. Methods

2.1. Computerized Models

Realistic 3D model for the atrial anatomy was composed of 284578 nodes and 1353783 tetrahedrons (673.4±130.3μm between nodes). To simulate the electrophysiological properties of atria, and consequently the electrical propagation patterns, a gradient was introduced into the atrial cell formulation ($I_{k,ACH}$, I_{K1}, I_{Na}, and I_{CaL}). Fibrotic tissue was modeled by disconnecting a certain percentage of nodes depending on the pattern to simulate. The system of differential equations was solved by using Runge–Kutta integration (using NVIDIA Tesla C2075 6G). Final computerized models were composed of N=2048 nodes for atria and M=659 for torso, under the assumption of a homogenous, unbounded, and quasi-static conducting medium by summing up all effective dipole contributions over the entire model [44, 40, 18, 20].

This geometrical model considers a simplified single endocardium-epicardium layer for the atrial tissue. Atria and torso models were used to simulate four different types of propagation patterns with a duration of 4 seconds, namely:

- *Normal sinus rhythm (SR)*: atrial tissue activated at 1.2 Hz.

- *Right atrial appendage (RAA)-located driver model*: with a single functional re-entry located at the RAA, which rotates at 5 Hz, while the remaining of the atrial tissue is activated at 3.1 Hz.

- *Two stable drivers (Two rotors, TR)*: a more complicated computational model with two stable drivers in Posterior Left Atrial Wall (PLAW) and in Superior Right Atrial Wall (SRAW). This model also contains two anatomical re-entries close to the left pulmonary veins and the right inferior pulmonary vein. In this case, the atrial tissue is activated between 6 and 7 Hz.

- *Left superior pulmonary vein (LSPV)-located driver model*: with 50% of atrial cells under fibrotic conditions and a single functional re-entry located close to the LSPV, rotating at 7.8 Hz,while the remaining of the atrial tissue is activated between 3 and 6.5 Hz.

2.2. Epicardial potentials estimation

We assume that the estimation of epicardial potentials follows the following linear model:

$$y_t = Ax_t + \epsilon,$$

where ϵ represents the model residuals. The goal of ECGI problem is to estimate epicardial potentials x_t using information from BSP, y_t, at time t, using the transfer matrix A. This is an ill-posed problem, which is commonly addressed with regularization.

2.2.1. Classical Tikhonov regularization (Tikh)

Tikhonov method is one of the most employed regularization methods in linear inverse problems. Tikhonov regularization is commonly used in linear inverse problems to stabilize the solution by penalizing its complexity. To estimate epicardial potentials x_t at time t, the function to minimize is:

$$\|y_t - Ax_t\|_2^2 + \lambda_1 \|Lx_t\|_2^2 \tag{1}$$

where λ_1 is the global regularization parameter, and L is a $N \times N$ matrix. The matrix L can take several forms. If L takes the identity matrix form, the solution is constrained in energy norm (zero-order Tikhonov, L_2-norm of the solution is minimized). However, if L takes the form of the first (surface gradient operator) or second spatial derivative (surface Laplacian operator), the solution is constrained to have a smooth surface gradient (first-order Tikhonov) or curvature (second-order Tikhonov), respectively [38, 6]. For this study we used zero-order Tikhonov method, which is the standard method and gives good results [18].Computing λ_1 for each time instant does not improve significantly the results compared to using a global regularization parameter for all the time instants, which needs much more computation time. [18].

The closed-form solution is:

$$\hat{x}_t = \left(A^T A + \lambda_1 L^T L \right)^{-1} A^T y_t \tag{2}$$

2.2.2. Constrained Tikhonov regularization (Cons-Tikh)

In this work, we will take into account endocardial information from intracavitary EGMs. We propose to incorporate this information, as an additional constraint, in the Tikhonov formulation, as:

$$\left\| \boldsymbol{y}_t - \boldsymbol{A}\boldsymbol{x}_t \right\|_2^2 + \lambda_1 \left\| \boldsymbol{L}\boldsymbol{x}_t \right\|_2^2 + \lambda_2 \left\| \boldsymbol{D}\boldsymbol{x}_{ref} - \boldsymbol{D}\boldsymbol{x}_t \right\|_2^2 \quad (3)$$

where $\boldsymbol{D}$ is a diagonal matrix with value equal to one for nodes where the solution is forced to be be similar to the selected measured endocardial potentials (allowing a controlled error). The vector $\boldsymbol{x}_{ref}$ represents the EGM signals recorded in the endocardium. Thus, this constraint controls the size of the error between reconstructed potentials ($\boldsymbol{x}_t$) and the known intracavitary signals ($\boldsymbol{x}_{ref}$). The proposed approach can be solved with a closed-form solution:

$$\hat{\boldsymbol{x}}_t = \left(\boldsymbol{A}^T \boldsymbol{A} + \lambda_1 \, \boldsymbol{L}^T \boldsymbol{L} + \lambda_2 \boldsymbol{D}^T \boldsymbol{D} \right)^{-1} \left(\boldsymbol{A}^T \boldsymbol{y}_t + \lambda_2 \boldsymbol{D}^T \boldsymbol{x}_{ref} \right) \quad (4)$$

In contrast to Tikh, Cons-Tikh algorithm used in this study is a first-order Tikhonov-based method, since it provides a better performance and lower dispersion than zero and second-order ones [52].

2.2.3. Interpolation

By using endocardial recordings, an alternative approach to estimate the electrical activity in the whole atrial surface would be to interpolate intracavitary EGMs. In our study, we used interpolation methods using measured endocardial potentials ($\boldsymbol{x}_{ref}$) as known information. This allows us to establish a comparison against Classical Tikhonov and Constrained Tikhonov (Cons-Tikh). We used an approach based on Laplacian interpolation, where the Laplacian is minimized at all nodes [37]. This method uses the geometry of the mesh to interpolate, while other cloud-point based methods are only distance-based methods.

2.3. Performance metrics

To assess the performance of the implemented reconstruction methods several metrics were used. Similarity between modeled and estimated $\hat{\boldsymbol{x}}$ epicardial potentials and phase maps is quantified by the relative difference measurement star (RDMS) [30] and, Pearson's correlation coefficient (CC), both across all nodes [18, 21]. RDMS is computed as:

$$RDMS = \sqrt{\sum_k \left(\frac{x_k}{\|\boldsymbol{x}\|_2} - \frac{\hat{x}_k}{\|\hat{\boldsymbol{x}}\|_2} \right)^2} \quad (5)$$

where k runs through all cardiac nodes.

We also computed Local Activation Times (LAT) for each model, and computed both RDMS and CC metrics between ground truth and the different reconstruction methods [11].

2.4. Dominant Frequency Analysis

Spectral analysis of cardiac electrical activity, and specifically the estimation of the dominant frequency (DF), has been previously proposed as an useful clinical tool for driver localization to guide ablation procedures [23, 2, 40]. To estimate DFs in each node, Welch's periodogram was computed to perform a frequency analysis (2s Hamming window, 50% overlap). Then, we used a signal preprocessing according to the bandpass nature of the EGM spectral envelope [35, 3, 8]. We also corrected wrong determinations of second or third harmonic peaks as DF [23].

2.5. Phase maps and Driver location

Phase maps are used to detect the core of the re-entrant activity [22, 46]. In order to estimate driver position, we computed phase maps by applying a Hilbert transform to the epicardial potentials [18]. Phase maps obtained using reconstructed epicardial potentials are compared with ground truth using both RDMS and CC, similarly to epicardial potential maps.

Phase maps were computed with the main aim of detecting Phase Singularities (PS). A PS is defined as the point in a phase map that is surrounded by phases from 0 to 2π. Only those PSs that, at least, last two full rotations were considered [43]. Using this approach, for each point in the atria it is possible to detect none, one or even more PSs for each time instant.

However, PSs estimations have both technical and structural limitations [41, 32], since there are PSs that seem to be primary drivers, and other PSs can be secondary drivers or spurious effects of the analysis [44]. To identify areas where PSs correspond to primary drivers, we only focus on those PSs that appear on high DF zones [46, 45].

To evaluate PS locations into a certain time interval, we used the PS Spatial Mass Function (SMF), which is a probability map of the position of PSs. To estimate the PS-SMF, we counted the number of times that a PS appears in a certain node over a given time interval, and then computed the subsequent probability over the whole number of time intervals. Therefore, the higher the probability of finding a driver in a certain node, the higher the probability of considering that area as an AF driver.

Finally, to compare the position of PSs between ground truth and estimations, we used the weighted under-estimation and over estimation indicators (WUI and WOI, respectively), which are weighted versions of the ones proposed in [54], the correlation coefficient between the histograms of the spatial mass function of the PS location (CC_{SMF}), and the mode distance (MD), defined as the Dijkstra distance between the modes of the ground truth and the estimated SMFs [18].

2.6. Experimental set-up

The forward problem was solved by computing the $M \times N$ transfer matrix $\mathbf{A}$ using the boundary element method [40, 4, 15]. Simulated BSP were referenced to the Wilson Terminal Center, corrupted with additive Gaussian noise (SNR =
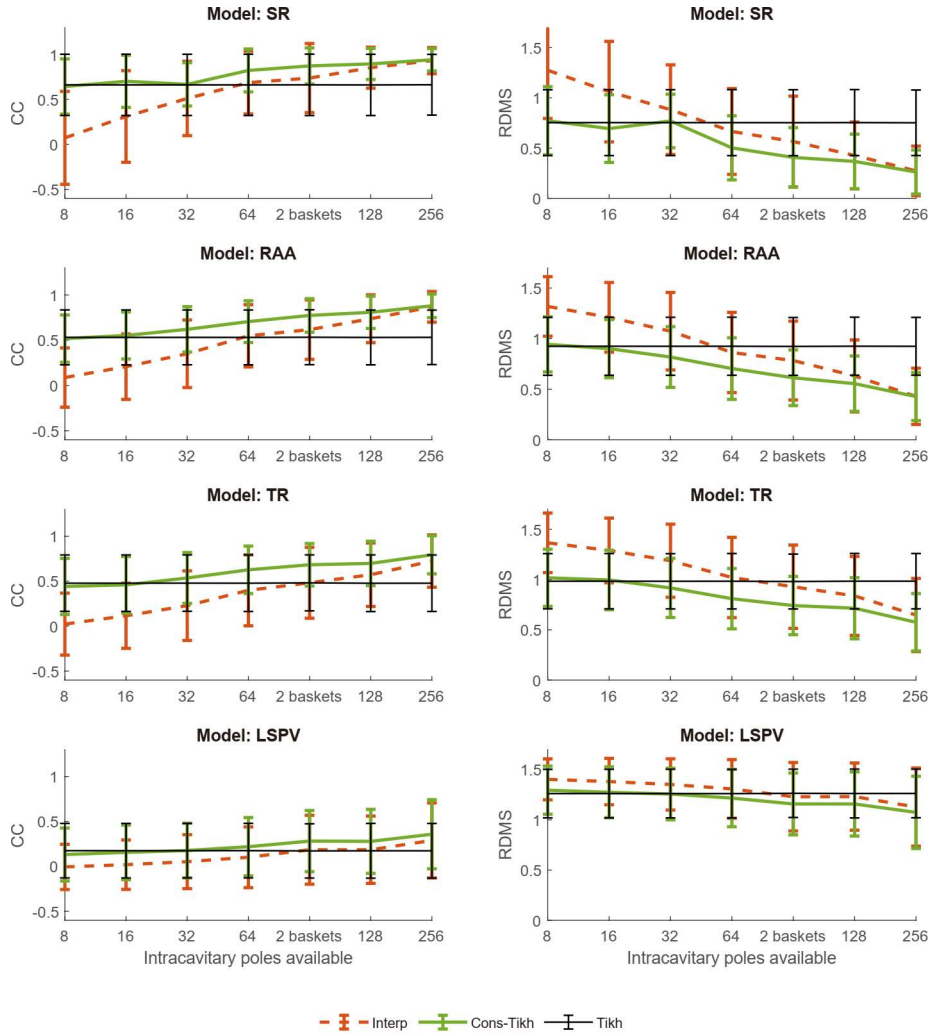
Figure 1: Performance assessment of interpolation, Tikh and Cons-Tikh algorithms, with different number of known nodes. 2 64-pole baskets-based distribution gives a similar global performance as 128 uniformly distributed nodes in Cons-Tikh algorithm.

20 dBs) and filtered using: 4th-order bandpass Butterworth filter (fc_1=3 Hz and fc_2=30Hz for AF models, fc_1=0 Hz and fc_2=30Hz for SR) [40, 18]. To obtain regularization parameters for Tikh (λ_1) we used the L-Curve method [40, 53, 18, 44], while in Cons-Tikh (λ_1, λ_2), we used a 3D-generalization of the L-Curve (L-surface) [5].

One of the main objectives is to study the impact of the number of intracavitary known nodes in the reconstruction. We compared results in a range of 8 up to 256 known nodes (in powers of two), uniformly and equispaced distributed across the atria. We also compared results with a more realistic distribution of nodes based on a simulation of two basket catheters with 64 poles, given a total of 128 known nodes, realistically distributed. In both cases, intracavitary electrodes are assumed to be in contact with the endocardial surface.

2.7. Real data

We used data from one (EPS) available at the Experimental Data and Geometric Analysis Repository (EDGAR).

The EPS was recorded at the Gregorio Marañón General University Hospital, Madrid, Spain, in collaboration with the Universitat Politècnica de València, València, Spain. It contains recordings from one male patient admitted for ablation of drug-refractory paroxysmal AF, using an ablation protocol approved by the Institutional Ethics Committee, and the patient gave informed consent [40].

BSP signals were recorded simultaneously to right-atrial endocardial recordings with high-resolution multipolar catheters. To obtain atrial signals without ventricular activity, an adenosine bolus infusion that blocked the atrio-ventricular node was used. This dataset contains one adenosine episode of 7.5 seconds.

Both EGMs and BSP were detrended and filtered using a 6th-order low-pass Butterworth filter (fc=30Hz). Inverse problem was performed using the same methodology as previous models, and DFs were estimated after performing a frequency analysis using a Welch's periodogram (1s Hamming window, 50% overlap). Finally, we computed the Root Mean Square Error (RMSE) between the DF of the given
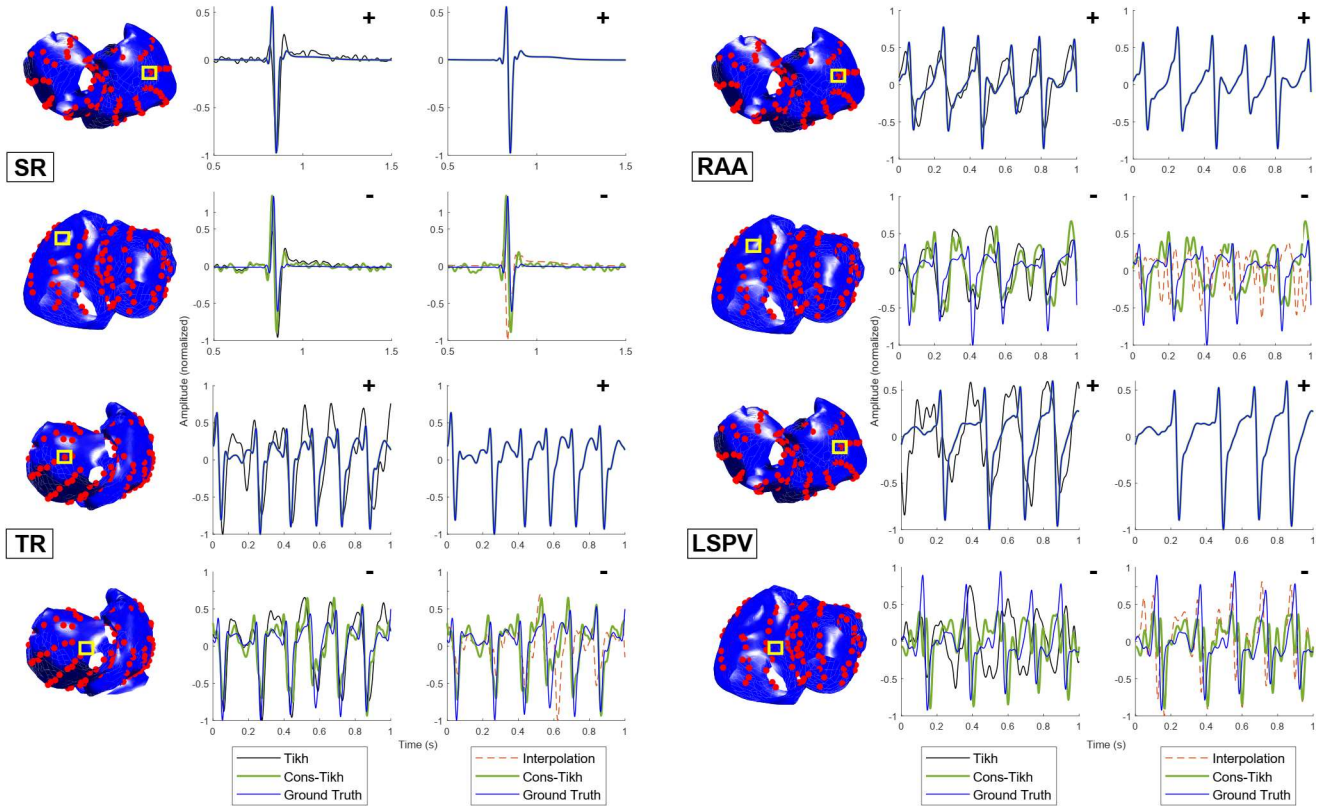
Figure 2: Clinical distribution of 128 nodes (2 64-pole baskets) across the atria, with reconstructed signals in a node used in the constraint of the Cons-Tikh algorithm (+) and a node not used in the constraint of the Cons-Tikh algorithm (-), using SR, RAA, TR and LSPV models.

Table 1
Epicardial estimation performance for SR, RAA, TR and LSPV models for SNR=20 dB and two intracavitary baskets: mean and standard deviation for RDMS and CC with interpolation, Tikh and Cons-Tikh methods.

	SR		*RAA*		*TR*		*LSPV*	
	RDMS	CC	RDMS	CC	RDMS	CC	RDMS	CC
Interpolation	0.57 ± 0.45	0.74 ± 0.38	0.80 ± 0.39	0.60 ± 0.33	0.93 ± 0.41	0.48 ± 0.39	1.23 ± 0.34	0.19 ± 0.38
Tikh	0.75 ± 0.33	0.66 ± 0.34	0.93 ± 0.28	0.53 ± 0.30	0.98 ± 0.27	0.48 ± 0.31	1.26 ± 0.24	0.17 ± 0.30
Cons-Tikh	0.41 ± 0.30	0.87 ± 0.20	0.63 ± 0.27	0.76 ± 0.18	0.74 ± 0.29	0.68 ± 0.24	1.16 ± 0.31	0.28 ± 0.34

EGMs and the corresponding inverse-problem reconstructions.

3. Results

3.1. Dependence on the number of known nodes

Epicardial potentials were estimated using interpolation, Tikh and the proposed model Cons-Tikh, for each propagation pattern. Figure 1 shows the mean and standard deviation of the CC (left) and RDMS (right) for different amounts of known nodes. Performance of Tikh is independent on the amount of intracavitary recordings available since it does not employ this information for the resolution.

For a small number of EGMs (between 8 and 32) inter-polation obtained higher RDMS and smaller CC values than Tikh and Cons-Tikh, which use BSP information. It means that interpolation yielded higher error when reconstructing epicardial signals. Indeed, for 8 known nodes, Cons-Tikh performed equal to Tikh, since the regularization parameter for intracavitary information, which weights the constraint effect for that information, is too small.

From 32 up to 256 known nodes interpolation and Cons-Tikh obtained lower RDMS (higher CC) than classical Tikh. Using 64 known nodes, interpolation performed as Tikh, while Cons-Tikh started to give a significantly better performance with 32 known nodes. Moreover, Cons-Tikh obtained even lower RDMS and higher CC values than interpolation of nodes, combining BSP and intracavitary information. Be-
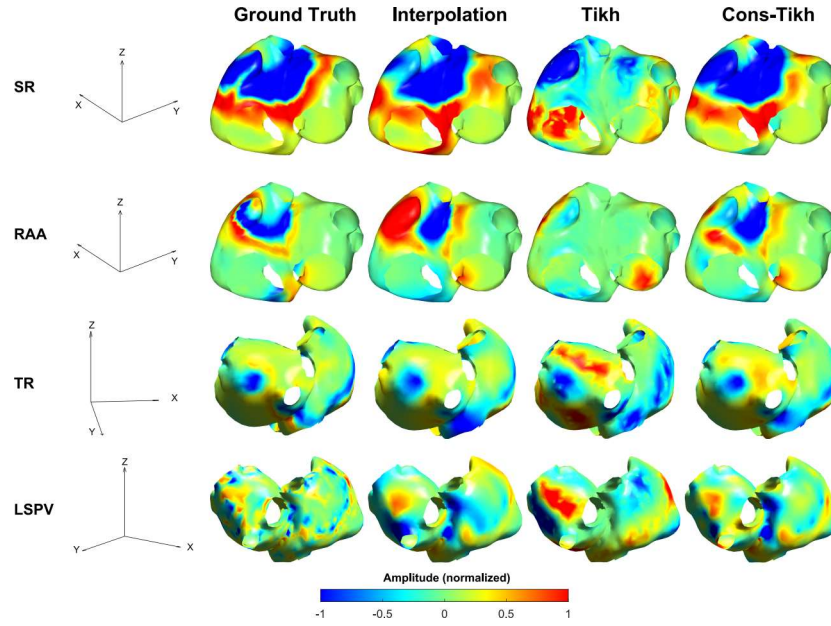
Figure 3: Comparison of model and estimated epicardial potential maps using interpolation, zero-order Tikh and first-order Cons-Tikh methods, in SR, RAA, TR and LSPV models. Interpolation and Cons-Tikh reconstructions are computed with two intracavitary baskets.
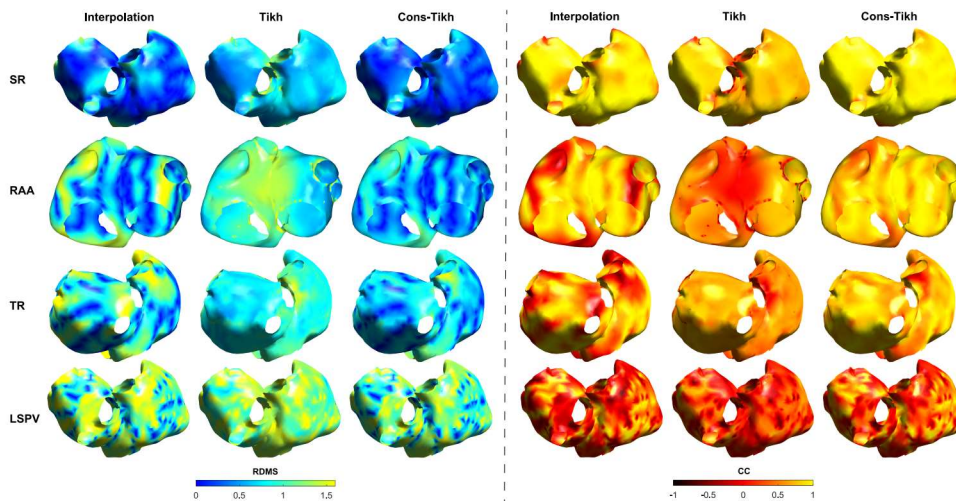
Figure 4: Comparison of error (assessed by RDMS, left) and similarity in the reconstructions (assessed by CC, right) maps across all nodes using interpolation, zero-order Tikh and first-order Cons-Tikh methods, in SR, RAA, TR and LSPV models. Interpolation and Cons-Tikh reconstructions are computed with two intracavitary baskets.

tween 32 and 256 known nodes, differences between interpolation and Tikh, and between interpolation and Cons-Tikh, were statistically significant ($p < 0.001$). However, differences in performance were smaller in complex AF patterns (like in LSPV model).

The same conclusion can be reached when using a clinical distribution of nodes (two intracavitary baskets). Numerical values for this scenario can be found in Table 1. Although the number of nodes is close to 128, the non-uniform distribution led to a slightly worse performance compared to 128 uniformly distributed nodes.

3.2. Performance with 2-64 pole basket-based distribution

In this section, we used a basket-model of two 64-poles intracavitary catheters. In such scenario, intracavitary information is restricted in some areas of the atria due to the anatomical limitations of any catheter.

Figure 2 shows the atrial model with two intracavitary baskets, with the EGMs obtained with interpolation and inverse problem solutions in different nodes for SR, RAA, TR and LSPV models, respectively. One of the main advantages of the proposed method is that, even in nodes not used as
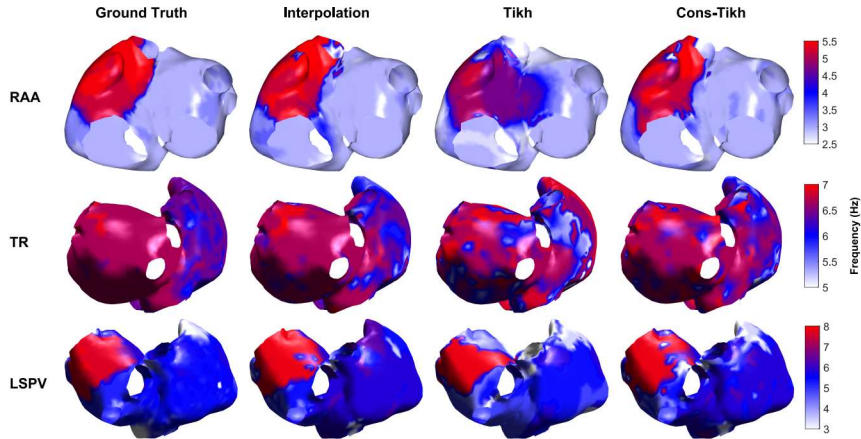
Figure 5: Comparison of model and estimated DF maps using interpolation, zero-order Tikh and first-order Cons-Tikh methods in RAA, TR and LSPV models. Interpolation and Cons-Tikh reconstructions are computed with two intracavitary baskets.
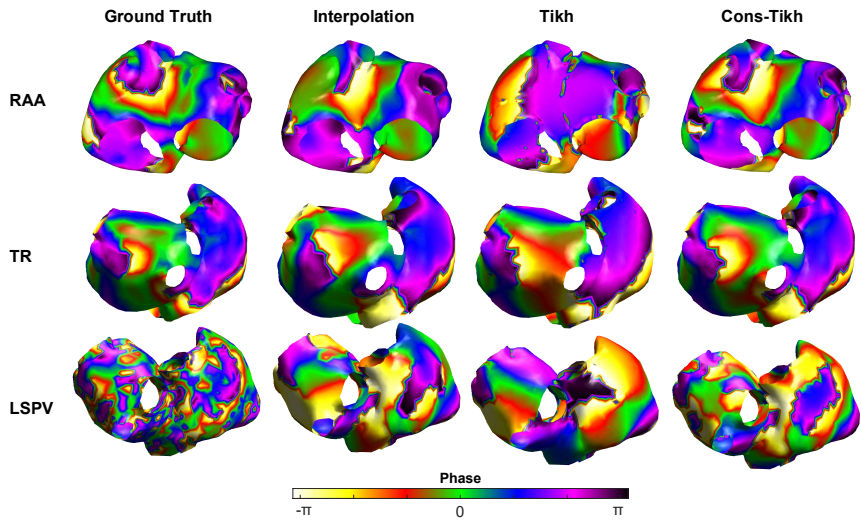
Figure 6: Comparison of model and estimated phase maps using interpolation, zero-order Tikh and first-order Cons-Tikh methods, in RAA, TR and LSPV models. Interpolation and Cons-Tikh reconstructions are computed with two intracavitary baskets.

a constraint, estimated epicardial potentials maintained the high-frequency content of the original signal, reducing the low-pass filtering behavior that Tikh imposes on the signal.

As the complexity of AF patterns increases, interpolation and Cons-Tikh performance degraded, with signal amplitude and phase changes comparing with the original signal. However, Cons-Tikh tended to perform slightly better than interpolation, since it uses both local and global information (endocardium and BSP). These conclusions were supported with lower RDMS and higher CC, see Table 1.

Figure 3 compares model and reconstructed epicardial potential maps. Interpolation and Cons-Tikh performed similarly, but a higher definition is reached with Cons-Tikh. Propagation patterns were better estimated with interpolation and Cons-Tikh, both in SR, RAA and TR model. However, performance degraded in LSPV epicardial potentials estimation (mean RDMS was 1.23, 1.26 and 1.16, and mean CC was 0.19, 0.17 and 0.28 for interpolation, Tikh and Cons-Tikh,

respectively).

Nevertheless, it is essential to remark that the main objective of using this distribution of intracavitary signals is to evaluate the performance of each method in atrial regions that cannot be mapped with the intracavitary baskets, such as the right atrial appendage. This is an atrial region where it is common to find drivers [28]. Similar conclusions can be drawn from Figure 4, where RDMS and CC maps are shown. The error, in terms of RDMS, using Cons-Tikh and interpolation, was lower than using the classical Tikh, while CC values were higher, which was expected (mean RDMS was 0.80 and 0.63, and mean CC was 0.60 and 0.76 for interpolation and Cons-Tikh for RAA model, respectively). Moreover, Cons-Tikh allowed us to diminish the error obtained when using only interpolation. As stated before, this is especially important in areas where intracavitary electrodes are unable to access. In the case of the RAA model, the error obtained in the area of the right atrial appendage with inter-
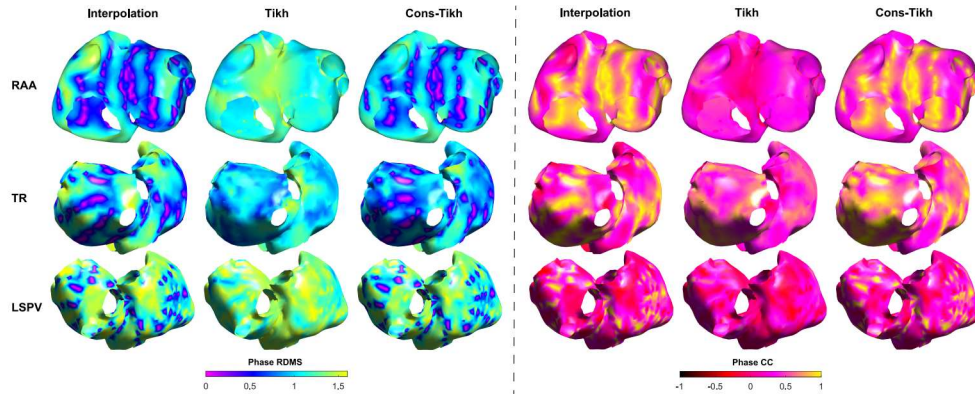
Figure 7: Comparison of error (assessed by RDMS, left) and similarity in the reconstructions (assessed by CC, right) in phase maps using interpolation, zero-order Tikh, and first-order Cons-Tikh methods, in RAA, TR and LSPV models. Interpolation and Cons-Tikh reconstructions are computed with two intracavitary baskets.

Table 2

Local activation times estimation performance for SR, RAA, TR and LSPV models for SNR=20 dB and two intracavitary baskets: mean RDMS and CC with interpolation, Tikh and Cons-Tikh methods.

	SR		*RAA*		*TR*		*LSPV*	
	RDMS	CC	RDMS	CC	RDMS	CC	RDMS	CC
Interpolation	0.10	0.99	0.17	0.99	0.20	0.98	0.76	0.71
Tikh	0.13	0.99	0.40	0.92	0.34	0.94	0.70	0.76
Cons-Tikh	0.08	0.99	0.15	0.99	0.27	0.96	0.68	0.76

polation was bigger than with Cons-Tikh. This result is also consistent with the RAA-model EGMs shown in Figure 2, where signals were better estimated with Cons-Tikh. Similar conclusions are obtained with TR model. If we focus on the areas that are not covered by intracavitary electrodes, the error using Cons-Tikh is also lower than using interpolation.

On the other hand, in the LSPV model, due to the higher complexity of the model, the areas where the error was minimal corresponded to zones close to the position of the known nodes, for both interpolation and Cons-Tikh.

Table 2 shows mean RDMS and CC of Local Activation Times (LAT) obtained with interpolation, Tikh and Cons-Tikh methods. Cons-Tikh provided reconstructions with lower RDMS (higher CC), suggesting better LAT estimations.

Figure 5 shows DF maps. Classical approach using Tikh led to poor estimations in some areas. In simple AF propagation patterns (RAA), DF estimation performance using both interpolation and Cons-Tikh was very similar. Cons-Tikh also allowed to reconstruct the DF map with high precision in the more complex LSPV pattern. It seems that the combination of intracavitary and BSP information allows to provide enough information to reconstruct high and low DF regions, even in TR model.

Figures 6 and 7 show phase and RDMS-CC phase maps, respectively. Since phase estimation relies mainly on the morphology of the signal, Cons-Tikh tended to provide better results (lower RDMS and higher CC), mainly in simple AF propagation patterns. Intracavitary information forced

the solution to take into account high frequency content in the EGMs, leading to a more accurate phase reconstruction.

3.3. Driver detection in a realistic scenario

One important clinical application of cardiac mapping is to locate sites of phase singularities (PS). Figure 8 shows the spatial mass function (SMF) of the PS location (i.e. probability map of the position of PSs). For every AF propagation pattern, interpolation was unable to obtain an accurate probability map of the position of PSs, underestimating both probabilities and areas where the driver could be found. Cons-Tikh was able to obtain a narrower and accurate area with high probability of finding a PS, compared to both interpolation and Tikh. In the case of RAA model, this result is consistent due to the lack of capability to correctly map electrical activity at the RAA. Moreover, in TR model, Cons-Tikh was able to estimate the presence of a primary driver (area with a higher probability of finding an PS) and a secondary driver (lower probability area, below the primary driver).

Table 3 shows the PS-detection performance metrics. Cons-Tikh yielded to smaller WUI and WOI than interpolation and Tikh methods, mainly in complex propagation patterns (with WUI = 35,46% and 30.03%, and WOI = 12.64% and 19.39% for TR and LSPV models using Cons-Tikh, respectively). Therefore, reconstructions with Cons-Tikh led to lower rate of false negatives and false positives. In terms of MD, Cons-Tikh gave lower values, namely in LSPV model. This result
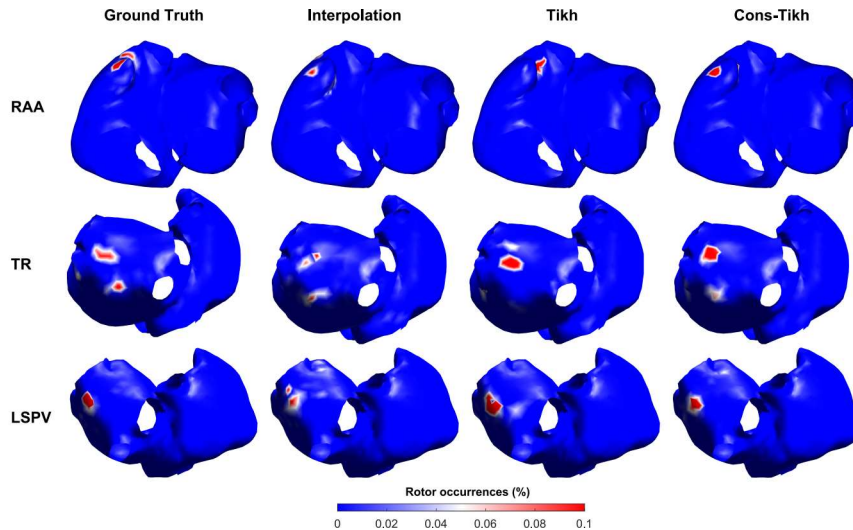
Figure 8: Spatial mass function (SMF) of the PS location, in RAA, TR and LSPV models using original model, Tikh and Cons-Tikh. Interpolation and Cons-Tikh estimation are computed with two intracavitary baskets.

Table 3
PS estimation performance for RAA, TR and LSPV models for SNR=20 dB and two intracavitary baskets: correlation coefficient of spatial mass function of PS location (CC_{SMF}), WUI (%), WOI (%) and mode distance (MD).

	RAA				TR				LSPV			
	CC_{SMF}	WUI	WOI	MD	CC_{SMF}	WUI	WOI	MD	CC_{SMF}	WUI	WOI	MD
Interpolation	0	100	100	1.639	0.52	48.80	48.79	0.50	0.39	59.82	44.64	0.90
Tikh	0.11	4.70	95.79	0.98	0.62	44.34	13.58	0	0	100	100	15.88
Cons-Tikh	0.24	4.70	92.33	0.98	0.72	35.46	12.64	0	0.86	30.03	19.39	0

is also consistent with CC_{SMF} metrics, where Cons-Tikh SMF correlation with the ground truth was higher than both Tikh and interpolation (0.24, 0.72 and 0.86 for RAA, TR and LSPV models using Cons-Tikh, respectively). In the case of RAA model, where the driver was in a area difficult to map with intracavitary basket, all reconstruction methods worsened, but Cons-Tikh was still the best method to find the driver location (higher CC_{SMF}, and lower WUI, WOI and MD), showing that the combination of intracavitary information and BSPs information allowed to enhance the electrical map estimation, and allowed to better estimate clinical targets.

3.4. Patient data

Figure 9 shows DF maps for a real patient recording. The classical Tikh method led to a more smooth DF map than Cons-Tikh, which is in agreement with previous results in computerized models. We can compare DF estimations using the recorded EGMs. As expected, Cons-Tikh obtained DF estimations closer to the intracavitary estimations than Tikh in terms of mean root mean square error (mRMSE), namely mRMSE = 0.90 Hz for Tihk, while mRMSE = 0.65 Hz using Cons-Tikh.

We have performed a simple experiment in which we randomly removed one electrode from the constraint in Cons-Tikh. After that, we could estimate DF difference comparing with an intracavitary EGM which was not used in the reconstruction as a prior information. This allowed us to provide a more fair estimation of the DF error. We repeated the experiment 100 times. In this experiment, Cons-Tikh was better estimating DF with a mRMSE = 0.85 Hz (0.90 Hz with Tikh).

There still are some issues that have to be addressed in real data, namely different reference signal for intracavitary and EGMs and BSPs, or the selection of regularization parameters using L-surface and L-curve.

4. Discussion and conclusions

In this work, we propose a new method to include intracavitary information from endocardial EGMs into our ECGI inverse methodology. That is, we have included this information as a second constraint on the Tikhonov regularization method.

Using multiple constrains on the spatial and temporal behavior has been previously proposed to improve epicardial potentials reconstruction [38, 6]. In [51], a Bayesian-based approach to incorporate a priori information was analyzed with good results, but in a different clinical scenario, i.e.
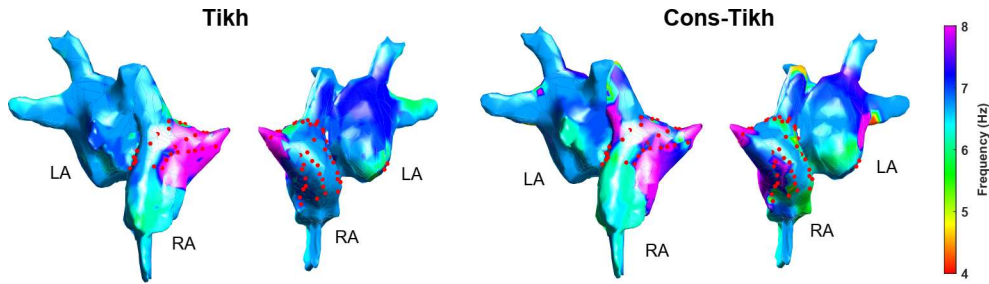
Figure 9: Comparison of estimated DF maps using zero-order Tikh (left) and first-order Cons-Tikh (right) methods in one real patient record. Left and right atria are denoted as LA and RA, respectively. Red dot points represent the position of the electrodes recording the intracavitary EGMs.

ventricular paced beats. In that work, authors included prior information by estimating the covariance matrix of epicardial potentials. This Bayesian approach has been studied in AF models with good results, but in order to estimate properly the covariance matrix all the intracavitary information was used ($\approx$ 2000 nodes) [18]. The method we propose was able to obtain more accurate reconstructions in AF with few nodes (64 nodes), see Figure 1.

Specifically, the proposed model improved the estimation of epicardial potentials by using first-order Constrained Tikhonov method, which is able to reproduce high frequency components in the solution. Therefore, this method overcomes the low-pass filtering behavior of the classical Tikhonov approach. Furthermore, Cons-Tikh clearly outperforms interpolation of nodes when we have less than 128 available nodes, obtaining lower RDMS (higher CC) values, although the epicardial potential estimation degraded severely for all the methods as the complexity of AF increases.

The proposed method has two free regularization parameters to be estimated, which makes it very computationally expensive. We diminished the computational cost by using an iterative method based on computing the optimal parameter by iterating on an under-sampled λ parameter array. Once the highest L-surface curvature area is found on the current iteration, the corresponding optimal λ section is found and up-sampled for the next iteration, forcing the algorithm to look for the optimal values only on that up-sampled section. This iterative algorithm stops when the difference between optimal λ values on consecutive iterations is below a certain threshold. For example, for 50 iterations and a threshold of 10^{-12}, computation time can be diminished from approximately 8 hours from the method used in [52] to 10 minutes.

In our results, L-surface method to estimate regularization parameters gave a higher weight to intracavitary measurements than BSP, although regularization parameter for Tikhonov constraint (λ_1) were similar in our approach and the classical one. We expected this result, as we are using the same intracardiac measurements used to compute the BSP as a priori information for the Cons-Tikh algorithm in computerized models. Therefore, one limitation of computerized model analysis is that it describes a simplistic scenario.

On the other hand, it is essential to remark that the scope of this paper is to assess the performance of this new algorithm in a controlled simplified environment. However, endocardium-epicardium bi-layer model approximations and model mismatch are issues that should be taken into account in further studies to obtain better performance in real situations. There are some studies that addressed endocardium-epicardium conduction, e.g. [50, 17], and model mismatch [6].

Moreover, in the case of patient data, further research is necessary, mainly by assessing new adapted methodologies to select both λ values in real data, facing the reference mismatch between BSP and intracavitary EGMs, and validating the proposed methodology on a higher number of real patient datasets. Regarding patient signal recording, combined BSP-EGM measurement could be easily achieved in a real environment, since several studies simultaneously recorded BSPs and endocardial EGMs [23]. Therefore, it is possible to integrate both types of signals in the proposed formulation in a clinical setting.

Finally, another important point to discuss is the number of electrodes needed to improve classical zero-order Tikhonov regularization (without including intracardiac information). Currently, in clinical practice the number of endocardial electrodes is still small, e.g. PENTARAY™ catheter (Biosense Webster) composed of 20 poles [10]. However, the trend is to use catheters with a higher number of electrodes, i.e., Constellation™ [33] and Intellamap Orion™ (BostonScientific) [49] or FIRMap™ (Abbott Electrophysiology) [27], all of them with 64 poles. This trend would eventually allow obtaining reliable reconstructions using the Cons-Tikh approach, making this approach more attractive.

In summary, since the number of patients suffering from AF is constantly increasing, and the success of classical pulmonary vein isolation is failing in achieving long-term AF freedom, novel technologies to characterize AF continue being a clinical need. Our study demonstrates that the combination of intracardiac recordings and non-invasive ECGI mapping is a potential tool for a global detailed mapping of AF drivers.

Acknowledgements

CRediT authorship contribution statement

Miguel Ángel Cámara-Vázquez: Conceptualization; Methodology; Software; Data curation; Writing - original draft; Writing - review and editing. **Ismael Hernández-Romero:** Methodology; Software; Data curation. **Miguel Rodrigo:** Methodology; Software; Data curation. **Felipe Alonso-Atienza:** Conceptualization; Methodology; Software; Funding acquisition; Project administration. **Carlos Figuera:** Conceptualization; Methodology; Software; Funding acquisition; Project administration. **Eduardo Morgado-Reyes:** Writing - original draft; Writing - review and editing. **Felipe Atienza:** Conceptualization; Methodology; Data curation; Funding acquisition; Project administration. **María S. Guillem:** Conceptualization; Methodology; Data curation; Funding acquisition; Project administration; Writing - review and editing. **Andreu M. Climent:** Conceptualization, Methodology, Data curation, Funding acquisition, Project administration,Writing - review and editing. **Óscar Barquero-Pérez:** Conceptualization; Methodology; Software; Writing - original draft; Writing - review and editing.

References

[1] Annoni, E.M., Arunachalam, S.P., Kapa, S., Mulpuru, S.K., Friedman, P.A., Tolkacheva, E.G., 2018. Novel Quantitative Analytical Approaches for Rotor Identification and Associated Implications for Mapping. IEEE Transactions on Biomedical Engineering 65, 273–281. doi:10.1109/TBME.2017.2763460.

[2] Atienza, F., Almendral, J., Ormaetxe, J.M., Moya, Á., Martínez-Alday, J.D., Hernández-Madrid, A., Castellanos, E., Arribas, F., Arias, M.Á., Tercedor, L., Peinado, R., Arcocha, M.F., Ortiz, M., Martínez-Alzamora, N., Arenal, Á., Fernández-Avilés, F., Jalife, J., 2014. Comparison of radiofrequency catheter ablation of drivers and circumferential pulmonary vein isolation in atrial fibrillation. a noninferiority randomized multicenter radar-af trial. Journal of the American College of Cardiology 64, 2455–2467.

[3] Barquero-Pérez, Ó., Rojo-Álvarez, J.L., Caamaño, A.J., Goya-Esteban, R., Everss, E., Alonso-Atienza, F., Sánchez-Muñoz, J.J., García-Alberola, A., 2010. Fundamental frequency and regularity of cardiac electrograms with Fourier organization analysis. IEEE Transactions on Biomedical Engineering 57, 2168–2177. doi:10.1109/TBME.2010.2049574.

[4] Barr, R.C., Ramsey, M., Spach, M.S., 1977. Relating epicardial to body surface potential distributions by means of transfer coefficients based on geometry measurements. IEEE Transactions on biomedical engineering , 1–11.

[5] Belge, M., Kilmer, M.E., Miller, E.L., 2002. Efficient determination of multiple regularization parameters in a generalized L-curve framework. Inverse Problems 18, 1161–1183.

[6] Brooks, D.H., Ahmad, G.F., MacLeod, R.S., Maratos, G.M., 1999. Inverse electrocardiography by simultaneous imposition of multiple constraints. IEEE Trans. Biomed. Eng. 46, 3–18.

[7] Brooks, D.H., Macleod, R., 1997. Electrical imaging of the heart. IEEE Signal Process. Mag. 14, 24–42.

[8] Castells, F., Cervigón, R., Millet, J., 2014. On the Preprocessing of Atrial Electrograms in Atrial Fibrillation: Understanding Botteron's Approach. Pacing and Clinical Electrophysiology 37, 133–143. doi:10.1111/pace.12288.

[9] Chugh, S.S., Havmoeller, R., Narayanan, K., Singh, D., Rienstra, M., Benjamin, E.J., Gillum, R.F., Kim, Y.H., McAnulty, J.H., Zheng, Z.J., Forouzanfar, M.H., Naghavi, M., Mensah, G.A., Ezzati, M., Murray, C.J., 2014. Worldwide epidemiology of atrial fibrillation: A global burden of disease 2010 study. Circulation 129, 837–847. doi:10.1161/CIRCULATIONAHA.113.005119.

[10] Clermont Ferrand Centre, France, Andronache, M., Drca, N., Karolinska Institute, Sweden, Viola, G., San Francesco Hospital, Italy, 2019. High-resolution Mapping in Patients with Persistent Atrial Fibrillation: A Case-based Review of the PENTARAY™ Catheter. Arrhythmia & Electrophysiology Review 8, 1–10. doi:10.15420/aer.2019.8.3.S1.

[11] Cluitmans, M.J., Clerx, M., Vandersickel, N., Peeters, R.L., Volders, P.G., Westra, R.L., 2017. Physiology-based regularization of the electrocardiographic inverse problem. Medical & biological engineering & computing 55, 1353–1365.

[12] Cuculich, P.S., Wang, Y., Lindsay, B.D., Faddis, M.N., Schuessler, R.B., Damiano, R.J., Li, L., Rudy, Y., 2010. Noninvasive characterization of epicardial activation in humans with diverse atrial fibrillation patternsclinical perspective. Circulation 122, 1364–1372. doi:10.1161/CirculationAHA.110.945709.

[13] van Dam, P.M., Oostendorp, T.F., Linnenbank, A.C., van Oosterom, A., 2009. Non-invasive imaging of cardiac activation and recovery. Annals of Biomedical Engineering 37, 1739–1756.

[14] De Greef, Y., Schwagten, B., Chierchia, G.B., de Asmundis, C., Stockman, D., Buysschaert, I., 2018. Diagnosis-to-ablation time as a predictor of success: early choice for pulmonary vein isolation and long-term outcome in atrial fibrillation: results from the Middelheim-PVI Registry. EP Europace 20, 589–595. doi:10.1093/europace/euw426.

[15] De Munck, J., 1992. A linear discretization of the volume conductor boundary integral equation using analytically integrated elements. IEEE Transactions on Biomedical Engineering 39, 986–990.

[16] Dubois, R., Shah, A.J., Hocini, M., Denis, A., Derval, N., Cochet, H., Sacher, F., Bear, L., Duchateau, J., Jais, P., Haissaguerre, M., 2015. Non-invasive cardiac mapping in clinical practice: Application to the ablation of cardiac arrhythmias. Journal of Electrocardiology 48, 966–974. doi:10.1016/j.jelectrocard.2015.08.028.

[17] Erem, B., Coll-Font, J., Orellana, R.M., Št, P., Brooks, D.H., et al., 2013. Using transmural regularization and dynamic modeling for noninvasive cardiac potential imaging of endocardial pacing with imprecise thoracic geometry. IEEE transactions on medical imaging 33, 726–738.

[18] Figuera, C., Suárez-Gutiérrez, V., Hernández-Romero, I., Rodrigo, M., Liberos, A., Atienza, F., Guillem, M.S., Barquero-Pérez, Ó., Climent, A.M., Alonso-Atienza, F., 2016. Regularization Techniques for ECG Imaging during Atrial Fibrillation: A Computational Study. Frontiers in Physiology 7, 466. doi:10.3389/fphys.2016.00466.

[19] Fuster, V., Rydén, L.E., Cannom, D.S., Crijns, H.J., Curtis, A.B., Ellenbogen, K.A., Halperin, J.L., 2006. Acc/aha/esc 2006 guidelines for the management of patients with atrial fibrillation: full text. Europace 8, 651–745. doi:10.1093/europace/eul097.

[20] García-Molla, V., Liberos, A., Vidal, A., Guillem, M., Millet, J., González, A., et al., 2014. Adaptive step {ODE} algorithms for the 3d simulation of electric heart activity with graphics processing units. Computers in Biology and Medicine 44, 15 – 26.

[21] Gharbalchi, F., Serinagaoglu, Y., Wilhelm, G., 2014. Inverse Electrocardiography using Reduced Leadset by TTLS and LTTLS Regularization Algorithms. Recent Advances in Electrical Engineering , 134–140.

[22] Guillem, M., Climent, A., Rodrigo, M., Fernández-Avilés, F., Atienza, F., Berenfeld, O., 2016. Presence and stability of rotors in atrial fibrillation: evidence and therapeutic implications. Cardiovascular Res. 109, 480–492.

[23] Guillem, M.S., Climent, A.M., Millet, J., Arenal, Á., Fernández-Avilés, F., Jalife, J., Atienza, F., Berenfeld, O., 2013. Noninvasive localization of maximal frequency sites of atrial fibrillation by body surface potential mapping. Circulation: Arrhythmia and Electrophysiology 6, 294–301.

[24] Gulrajani, R., 1998. The forward and inverse problems of electrocardiography. IEEE Eng. Med. Biol. 17, 84–101.

[25] Haissaguerre, M., Hocini, M., Denis, A., Shah, A.J., Komatsu, Y., Yamashita, S., et al., 2014. Driver domains in persistent atrial fibrillation. Circulation 130, 530–538.

[26] Haissaguerre, M., Hocini, M., Shah, A.J., Derval, N., Sacher, F., Jais, P., Dubois, R., 2013. Noninvasive panoramic mapping of human atrial fibrillation mechanisms: A feasibility report. Journal of Cardiovascular Electrophysiology 24, 711–717.

[27] Krummen, D.E., Baykaner, T., Schricker, A.A., Kowalewski, C.A., Swarup, V., Miller, J.M., Tomassoni, G.F., Park, S., Viswanathan, M.N., Wang, P.J., Narayan, S.M., 2017. Multicentre safety of adding Focal Impulse and Rotor Modulation (FIRM) to conventional ablation for atrial fibrillation. Europace 19, 769–774. doi:10.1093/europace/euw377.

[28] Lim, H.S., Hocini, M., Dubois, R., Denis, A., Derval, N., Zellerhoff, S., Yamashita, S., Berte, B., Mahida, S., Komatsu, Y., et al., 2017. Complexity and distribution of drivers in relation to duration of persistent atrial fibrillation. Journal of the American College of Cardiology 69, 1257–1269. doi:10.1016/j.jacc.2017.01.014.

[29] MacLeod, R.S., Brooks, D.H., 1998. Recent progress in inverse problems in electrocardiology. Biol. Soc. Magazine 17, 73 – 83.

[30] Meijs, J.W., Weier, O., Peters, M.J., van Oosterom, A., 1989. On the numerical accuracy of the boundary element method (EEG application). IEEE Transactions on Biomedical Engineering 36, 1038–1049. doi:10.1109/10.40805.

[31] Milanic, M., Jazbinsek, V., MacLeod, R.S., Brooks, D.H., Hren, R., 2014. Assessment of regularization techniques for electrocardiographic imaging. Journal of Electrocardiology 47, 20 – 28.

[32] Mohanty, S., Gianni, C., Trivedi, C., Metz, T., Bai, R., Al-Ahmad, A., Bailey, S., Burkhardt, J.D., Gallinghouse, G.J., Horton, R., Hranitzky, P.M., Sanchez, J.E., Di Biase, L., Natale, A., 2018. Impact of rotor ablation in non-paroxysmal AF patients: Findings from the per-protocol population of the OASIS trial at long-term follow-up. American Heart Journal 205, 145–148. doi:10.1016/j.ahj.2018.05.021.

[33] Narayan, S.M., Krummen, D.E., Shivkumar, K., Clopton, P., Rappel, W.J., Miller, J.M., 2012. Treatment of Atrial Fibrillation by the Ablation of Localized Sources. Journal of the American College of Cardiology 60, 628–636. doi:10.1016/j.jacc.2012.05.022.

[34] Navara, R., Leef, G., Shenasa, F., Kowalewski, C., Rogers, A.J., Meckler, G., Zaman, J.A.B., Baykaner, T., Park, S., Turakhia, M.P., Zei, P., Viswanathan, M., Wang, P.J., Narayan, S.M., 2018. Independent mapping methods reveal rotational activation near pulmonary veins where atrial fibrillation terminates before pulmonary vein isolation. Journal of Cardiovascular Electrophysiology 29, 687–695. doi:10.1111/jce.13446.

[35] Ng, J., Kadish, A.H., Goldberger, J.J., 2007. Technical considerations for dominant frequency analysis. Journal of Cardiovascular Electrophysiology 18, 757–764. doi:10.1111/j.1540-8167.2007.00810.x.

[36] Oesterlein, T., Frisch, D., Loewe, A., Seemann, G., Schmitt, C., Dössel, O., Luik, A., 2016. Basket-Type Catheters: Diagnostic Pitfalls Caused by Deformation and Limited Coverage. BioMed research international 2016, 5340574. doi:10.1155/2016/5340574.

[37] Oostendorp, T., Oosterom, A., Huiskamp, G., 1989. Interpolation on a triangulated 3d surface. Journal of Computational Physics 80, 331–343.

[38] Oster, H.S., Rudy, Y., 1992. The use of temporal information in the regularization of the inverse problem in electrocardiography. IEEE Trans. Biomed. Eng. 39, 65–75.

[39] Pedron-Torrecilla, J., Climent, A., Millet, J., Berne, P., Brugada, J., Brugada, R., Guillem, M., 2011. Characteristics of inverse-computed epicardial electrograms of brugada syndrome patients, in: Engineering in Medicine and Biology Society, EMBC, 2011 Annual International Conference of the IEEE, pp. 235–238.

[40] Pedrón-Torrecilla, J., Rodrigo, M., Climent, A., Liberos, A., Pérez-David, E., Bermejo, J., et al., 2016. Noninvasive estimation of epicardial dominant high-frequency regions during atrial fibrillation. J. Cardiovascular Electrophysiol. 27, 435–442.

[41] Podziemski, P., Zeemering, S., Kuklik, P., van Hunnik, A., Maesen, B., Maessen, J., Crijns, H.J., Verheule, S., Schotten, U., 2018. Rotors Detected by Phase Analysis of Filtered, Epicardial Atrial Fibrillation Electrograms Colocalize With Regions of Conduction Block. Circulation: Arrhythmia and Electrophysiology 11. doi:10.1161/CIRCEP.117.005858.

[42] Potyagaylo, D., Loewe, A., Van Dam, P., Dössel, O., Dam, P.V., Olaf, D., 2016. ECG Imaging of Focal Atrial Excitation: Evaluation in a Realistic Simulation Setup. 2016 Computing in Cardiology Conference (CinC) , 113–116.

[43] Rodrigo, M., Climent, A.M., Liberos, A., Calvo, D., Fernández-Avilés, F., Berenfeld, O., et al., 2016. Identification of dominant excitation patterns and sources of atrial fibrillation by causality analysis. Annals of Biomedical Engineering 44, 2364–2376.

[44] Rodrigo, M., Climent, A.M., Liberos, A., Fernández-Avilés, F., Berenfeld, O., Atienza, F., Guillem, M.S., 2017a. Technical considerations on phase mapping for identification of atrial reentrant activity in direct- and inverse-computed electrograms. Circulation: Arrhythmia and Electrophysiology 10. doi:10.1161/CIRCEP.117.005008.

[45] Rodrigo, M., Climent, A.M., Liberos, A., Fernández-Avilés, F., Berenfeld, O., Atienza, F., Guillem, M.S., 2017b. Highest dominant frequency and rotor positions are robust markers of driver location during noninvasive mapping of atrial fibrillation: A computational study. Heart Rhythm 14, 1224–1233. doi:10.1016/j.hrthm.2017.04.017.

[46] Rodrigo, M., Guillem, M.S., Climent, A.M., Pedrón-Torrecilla, J., Liberos, A., Millet, J., et al., 2014. Body surface localization of left and right atrial high-frequency rotors in atrial fibrillation patients: A clinical-computational study. Heart Rhythm 11, 1584 – 1591.

[47] Rottner, L., Bellmann, B., Lin, T., Reissmann, B., Tönnis, T., Schleberger, R., Nies, M., Jungen, C., Dinshaw, L., Klatt, N., Dickow, J., Münkler, P., Meyer, C., Metzner, A., Rillig, A., 2020. Catheter Ablation of Atrial Fibrillation: State of the Art and Future Perspectives. Cardiology and Therapy 9, 45–58. doi:10.1007/s40119-019-00158-2.

[48] Rudy, Y., 2013. Noninvasive electrocardiographic imaging of arrhythmogenic substrates in humans. Circ. Res. 112, 863–874. doi:10.1161/circresaha.112.279315.

[49] Schaeffer, B., Hoffmann, B.A., Meyer, C., Akbulak, R.O., Moser, J., Jularic, M., Eickholt, C., Nührich, J.M., Kuklik, P., Willems, S., 2016. Characterization, mapping, and ablation of complex atrial tachycardia: Initial experience with a novel method of ultra high-density 3d mapping: Ultra high-density mapping of complex at. Journal of Cardiovascular Electrophysiology 27, 1139–1150. doi:10.1111/jce.13035.

[50] Schuler, S., Potyagaylo, D., Dössel, O., 2017. Ecg imaging of simulated atrial fibrillation: Imposing epi-endocardial similarity facilitates the reconstruction of transmembrane voltages, in: 2017 Computing in Cardiology (CinC), pp. 1–4.

[51] Serinagaoglu, Y., Brooks, D.H., Macleod, R.S., 2006. Improved performance of bayesian solutions for inverse electrocardiography using multiple information sources. IEEE Transactions on Biomedical Engineering 53, 2024–2034.

[52] Suárez-Gutiérrez, V., Cámara, M.A., Barquero-Pérez, O., Hernández, I., Guillem, M.S., Climent, A.M., Alonso-Atienza, F., Figuera, C., 2017. Including a priori knowledge in the solution of the inverse problem during atrial fibrillation. 44th Computing in Cardiology .

[53] Tikhonov, A.N., Arsenin, V.Y., 1977. Solutions of Ill-posed Problems. New York: Wiley.

[54] Wang, D., Kirby, R.M., MacLeod, R.S., Johnson, C.R., 2013. Inverse electrocardiographic source localization of ischemia: An optimization framework and finite element solution. Journal of Computational Physics 250, 403 – 424.